

HHS Public Access

Author manuscript

Ann Biomed Eng. Author manuscript; available in PMC 2018 December 01.

Published in final edited form as:

Ann Biomed Eng. 2017 December; 45(12): 2762-2774. doi:10.1007/s10439-017-1920-7.

Why are antagonist muscles co-activated in my simulation? A musculoskeletal model for analysing human locomotor tasks

Adrian K.M. Lai^{1,*}, Allison S. Arnold², and James M. Wakeling¹

¹Department of Biomedical Physiology and Kinesiology, Simon Fraser University, Burnaby, BC, Canada

²Department of Organismic and Evolutionary Biology, Concord Field Station, Harvard University, Bedford, MA, USA

Abstract

Existing "off-the-shelf" musculoskeletal models are problematic when simulating movements that involve substantial hip and knee flexion, such as the upstroke of pedalling, because they tend to generate excessive passive fibre force. The goal of this study was to develop a refined musculoskeletal model capable of simulating pedalling and fast running, in addition to walking, which predicts the activation patterns of muscles better than existing models. Specifically, we tested whether the anomalous co-activation of antagonist muscles, commonly observed in simulations, could be resolved if the passive forces generated by the underlying model were diminished. We refined the *OpenSim*TM model published by Rajagopal et al. (2016) by increasing the model's range of knee flexion, updating the paths of the knee muscles, and modifying the force-generating properties of eleven muscles. Simulations of pedalling, running and walking based on this model reproduced measured EMG activity better than simulations based on the existing model – even when both models tracked the same subject-specific kinematics. Improvements in the predicted activations were associated with decreases in the net passive moments; for example, the net passive knee moment during the upstroke of pedalling decreased from 36.9 N m (existing model) to 6.3 N m (refined model), resulting in a dramatic decrease in the co-activation of knee flexors. The refined model is available from SimTK.org and is suitable for analysing movements with up to 120° of hip flexion and 140° of knee flexion.

Key terms

musculoskeletal model; Hill-type muscle model; simulation; passive force; running; pedalling

Introduction

Muscle-driven simulations, based on rigid body models of musculoskeletal structures, offer a practical and appealing approach for estimating forces that cannot be measured non-invasively, such as *in-vivo* musculotendon forces (e.g. ^{14,22}) and joint contact forces (e.g. ¹¹) during walking and other movements. Over the past thirty years, detailed musculoskeletal

^{*}Address for correspondence: Department of Biomedical Physiology and Kinesiology, Simon Fraser University, 8888 University Drive, Burnaby, BC, Canada, V5A 1S6, Phone: +1(778) 782-8445, adrian_lai@sfu.ca.

models of the human lower extremity have been developed, iteratively refined, and widely shared, for example using the *OpenSim*TM ⁶ open-source simulation platform or other software. Typically, such models characterise the three-dimensional (3D) geometry of the bones, the kinematics of the joints, and the force-generating properties of the muscles for a generic subject. Force-generating properties of muscles are parameterised based on experimental data that scale a normalised Hill-type muscle model (e.g. ³⁴) to individual muscles. Thus, existing models generally reflect the "best-available" descriptions of the muscles' attachments, moment arms, fibre lengths, and physiological cross-sectional areas (PCSAs), averaged across specimens or subjects.

Over the years, as more comprehensive data sets describing the architecture (e.g. ³¹) and moment arms (e.g. ⁴) of muscles have been published, and as refined Hill-type models have been implemented (e.g. ²³), musculoskeletal models have been tested and improved. For example, the lower extremity model originally published by Delp et al. ⁷ was based on measurements from five cadaveric specimens ^{12,33}. An updated version of this model, published by Arnold et al. ³¹ incorporated measurements from twenty-one specimens and better characterised muscles' origin-to-insertion lengths and moment arms. A more recent version of the model published by Rajagopal et al. ²⁵ further updated the muscles' forcegenerating properties based on magnetic resonance (MR) images of twenty-four healthy young adults ¹⁵. However, even the most up-to-date musculoskeletal models still pose significant challenges to users who wish to simulate movements that involve substantial hip and knee flexion, as summarized below.

During many movements, such as the swing phase of running, the upstroke of pedalling, and the early drive phase of rowing, the hips and knees are flexed more than 90°. Existing lower extremity models have three major limitations when analysed over these ranges of motion. The most troubling limitation, perhaps, is that existing models greatly overestimate the passive fibre forces developed by the hip and knee extensors, most notably when the joints are flexed and the muscles are stretched. As acknowledged by Rajagopal et al.²⁵, these large passive forces can lead to anomalous compensatory muscle activity in muscle-driven simulations. Another limitation is that the 3D paths of some muscles are poorly represented over the ranges of hip and knee angles commonly achieved by subjects during running, pedalling, and other movements. For example, in the model published by Rajagopal et al.²⁵, the knee flexion moment arm of the lateral gastrocnemius is diminished, and the moment arm of the biceps femoris short head surprisingly switches from flexion to extension, when the knee is flexed outside the model's recommended 120° operating range. Yet another limitation is that the gastrocnemii and other muscles in these models become too short to generate active force during portions of the cycle that involve substantial hip and/or knee flexion. Thus, while many studies have used simulation-based approaches to gain valuable new insights into muscle function during walking (e.g. ²²), the limitations of existing models must be resolved before such approaches can be reliably applied to a broader range of tasks.

The overarching aim of this study was to develop a refined lower extremity model capable of producing plausible, muscle-driven simulations of fast running and pedalling, in addition to walking, from motion capture data and measured reaction forces. In particular, we sought to generate subject-specific simulations in which the predicted muscle activation patterns

faithfully reproduced each subject's measured EMG recordings while accurately tracking the subject's motion data. It has sometimes been presumed that the anomalous co-activation of antagonist muscles — commonly found in simulations of tasks involving high hip or knee flexion — is an unavoidable result of existing tracking algorithms, such as computed muscle control ²⁷. Here, we hypothesised that the anomalous co-activation of antagonist muscles could be reduced if the excessive passive forces generated by hip and knee extensors in the underlying model were diminished. To test this hypothesis, we made several important changes to the model published by Rajagopal et al.²⁵, and we demonstrated the value of these changes in three illustrative examples. The refined model is available from SimTK.org (https://simtk.org/projects/model-high-flex) and is suitable for generating muscle-driven simulations of movements involving up to 120° of hip flexion and 140° of knee flexion.

Methods

We made several refinements to the open-source model published by Rajagopal et al.²⁵ to resolve problems we encountered when attempting to generate high-fidelity simulations of fast running and pedalling. Briefly, the existing model published by Rajagopal et al. includes rigid body representations of the bones that reflect the dimensions of an averaged-sized adult male (mass: 75 kg, height: 170 cm). Adjacent bones are connected via joints, yielding a fullbody model with 37 degrees of freedom (DoF): 6 at the pelvis, 7 in each leg, and 17 in the torso and upper body. The model is driven by 80 Hill-type muscle-tendon units (MTUs) that generate moments about the lower limb joints and 17 ideal torque actuators that move the torso and upper body. Each MTU is massless and is modelled as a Hill-type actuator with a single contractile element ²³. The muscle fibre is represented by normalised active forcelength and force-velocity curves and a passive force-length curve; the tendon is represented by a normalised length-tension curve. These curves are scaled to each MTU's maximum isometric force, optimal fibre length, tendon slack length, and pennation angle at optimal fibre length. Parameters that specify the force-generating capacity of each MTU are based on published estimates of optimal fibre lengths and pennation angles from 21 cadaveric specimens ³¹ and on muscle volumes reconstructed from MR images of 21 young healthy subjects ¹⁵. In particular, the maximum isometric force of each MTU is based on an estimate of the muscle's physiological cross-sectional area (PCSA) and an assumed specific tension of 60 N/cm². As described by Rajagopal et al. ²⁵, the PCSA of each muscle was determined by dividing the muscle's volume by its optimal fibre length. The volume of each muscle was calculated as a fraction of the total volume of all the lower limb muscles, and these fractions were based on 3D reconstructions of the musculature from MR images, as published by Handsfield et al. ¹⁵. The total volume of all lower limb muscles in the model was estimated from a regression equation published by Handsfield et al. ¹⁵, also derived from MR images, which predicts lower limb muscle volume based on body mass and height. The optimal fibre length used to estimate each muscle's PCSA was based on measurements of raw fibre lengths and associated sarcomere lengths published by Ward et al. ³¹, assuming an optimal sarcomere length of 2.7 µm ²¹.

In the current study, we updated the tibiofemoral kinematics as well as relevant musculotendon paths and parameters, including tendon slack length and in some cases optimal fibre lengths, for 22 MTUs (11 per leg) in the model. We did not change the

muscles' maximum isometric forces. Additional details about our refined model and test simulations are provided below.

Modification of the model's knee kinematics and origin-to-insertion paths

To support simulation-based studies of pedalling and other tasks that involve high knee flexion, we increased the model's range of knee flexion from 120° to 140°, and we updated the origin-to-insertion paths of the knee muscles accordingly. We also resolved a discrepancy in how motions of the tibia relative to the femur were defined in two previous models ^{2,25}, both of which were based on the cadaveric measurements of tibiofemoral motions published by Walker et al.³⁰. In our refined model, as in both previous models, the coupled rotations and translations of the tibia with respect to the femur are defined as a function of knee flexion angle. The varus/valgus and internal/external rotations of the tibia as a function of knee flexion are identical in all three models; however, the translations of the tibia in our refined model are generally greater than those specified in Rajagopal et al.'s model when the knee is flexed more than about 60°.

After modifying the model's knee kinematics, we updated the attachment points and/or wrapping surfaces of several MTUs in the model so that the muscles' moment arms about the knee were more consistent with moment arms published in the literature with increasing knee flexion (Fig. 1 and Suppl. Fig. S1). For example, by making small adjustments to the cylindrical wrapping surface that constrains the path of the vastus lateralis over the distal femur, we prevented this MTU from passing through the femur when the knee was flexed more than about 130° (Fig. 1). We also modified, for example, the paths of the biceps femoris short head and the lateral gastrocnemius to prevent these MTUs from passing too close to the knee axis, and thus potentially generating a knee extension moment at extreme knee flexion angles (Fig. 1). Hereafter, our model with the modified knee kinematics and updated MTU paths — but with the same force-generating properties as specified by Rajagopal et al.²⁵ — will be referred to as the *intermediate* model.

Development of test simulations

We used OpenSimTM v3.3 ^{6,16} to generate subject-specific simulations of pedalling, fast running and walking that tracked experimental data from healthy adult subjects. The data that we tracked were previously collected for two different, larger studies. Both protocols are described in detail elsewhere ^{8,18} and are only briefly reviewed here. To achieve the aims of the current study, we conducted detailed analyses of two representative subjects.

To simulate pedalling, we tracked the kinematics of a highly-trained female cyclist (age: 32 years, mass: 63.5 kg, height: 167 cm) who pedalled at 80 RPM on a stationary bicycle (Indoor Trainer, SRM, Julich, Germany) at a constant average crank torque and power of 26 N m and 200 W, respectively. The 3D trajectories of 32 active LED markers, placed on the pelvis, lower limbs and pedals, were recorded at 100 Hz (Certus Optotrak, NDI, Waterloo, Canada). Reaction forces normal (i.e. ineffective) and radial (i.e. effective) to the crank were recorded bilaterally at 2000 Hz using clipless instrumented pedals (Powerforce, Radlabor, Freiburg, Germany) attached to rigid sandals. EMG signals were recorded from 10 lower limb muscles at 2000 Hz using bi-polar Ag/AgCl surface electrodes (10 mm diameter; 21

mm inter-electrode distance; Norotrode, Myotronics, Kent, WA, USA). EMG signals were collected from the gluteus maximus (GM), rectus femoris (RF), biceps femoris long head (BF), semitendinosus (ST), vastus lateralis (VL), vastus medius (VM), medial gastrocnemius (MG), lateral gastrocnemius (LG), soleus (SO) and tibialis anterior (TA). EMG signals were filtered using an EMG-specific wavelet analysis ²⁸ as described elsewhere ²⁹. Five crank cycles from a representative 20 second trial were extracted for simulation. The subject gave informed consent, and protocols were approved by the Institutional Review Boards at Simon Fraser University and Harvard University.

To simulate walking and running, we tracked the kinematics of one male participant (age: 26 years, mass: 77 kg, height: 185 cm) who walked and ran at steady-state speeds of 1.4 m s⁻¹ and 4 m s⁻¹, respectively. The 3D trajectories of 37 markers (6-14 mm diameter), placed on the pelvis and lower limbs, were tracked at 250 Hz (Qualisys, Gothenburg, Sweden). Ground reaction forces were recorded at 1500 Hz using an instrumented force-measuring treadmill (Tandem Treadmill, Advanced Mechanical Technology, Watertown, MA, USA). Whenever a single leg contacted both force plates simultaneously, a "force-stitching" algorithm was used to determine the resultant force and centre-of-pressure vectors from the two force plates ¹⁸. Five gait cycles for each condition were extracted from 20 second trials and used for simulation. The subject gave informed consent, and protocols were approved by the Institutional Review Boards at the University of Melbourne and the University of Queensland.

Initially, we generated subject-specific musculoskeletal models by scaling our *intermediate* model to each subject's anthropometric dimensions. We filtered the subjects' 3D marker trajectories and measured reaction forces using a 4th order, low-pass Butterworth filter with cut-off frequencies of 10 Hz and 15 Hz, respectively. For these simulations, we removed the torso and upper limb segments of the model, along with the corresponding actuators, and we adjusted the mass and inertial properties of the pelvis to account for these changes. We computed the joint kinematics and the net joint moments for each DoF using inverse kinematics and inverse dynamics (Fig. 2). We generated a refined set of kinematics, more dynamically consistent with the reaction force data, using OpenSim's residual reduction algorithm (RRA). The maximum root-mean-square errors (RMSE) between our inverse kinematics and RRA solutions were less than 1.2° (rotational DoF) and 1.1 cm (pelvis translations); the maximum errors were less than 2.1° and 1.9 cm, respectively. These errors are within the recommended tolerances for kinematics obtained from RRA ¹⁶. We used the subjects' measured reaction forces and smoothed kinematics from RRA as inputs to OpenSim's computed muscle control (CMC) algorithm, which used forward integration (time window = 0.015 s) and a feedback controller to solve for a set of muscle excitations that reproduced each subject's measured movement dynamics ²⁷. Muscle excitations were bounded between 0 (no excitation) and 1 (full excitation). The active and passive forces generated by each MTU were computed in accordance with the model's force-lengthvelocity properties. We set the maximum shortening velocity of each MTU to 15 l₀^m s⁻¹ consistent with previous simulations of walking and running (e.g. 1,19).

Modification of the muscles' passive force-generating properties

Careful examination of these initial simulations, generated using our *intermediate* model, revealed that eight MTUs generated "excessive" passive force during some portion of the crank/gait cycle. For example, during the upstroke of pedalling, the knee extensors generated a passive knee extension moment that was nearly three times the net joint moment determined from inverse dynamics. The problematic MTUs that we identified included the three compartments of the gluteus maximus, the three vasti, and the rectus femoris and soleus muscles.

To decrease the passive forces produced by these MTUs, particularly over the more extreme ranges of hip and knee flexion, we altered parameters that scale the normalised Hill-type muscle model ²³ to each MTU. In particular, we increased the tendon slack length of each MTU (Table 1) — but we limited these changes to be smaller than the expected variation reported by Rajagopal et al.²⁵ To estimate tendon slack lengths for the existing model, Rajagopal et al. used the mean measured fibre lengths and sarcomere lengths reported by Ward et al.³¹ to specify, for each MTU, a normalised fibre length and a corresponding tendon slack length at a "reference" pose, defined as the average pose of the cadaveric specimen in Ward et al.'s study (7° hip flexion, 2° hip abduction, 0° knee flexion, and 20° plantar flexion).

In our study, we inferred that the normalised fibre length of each problematic MTU was likely too long at this reference pose. Given a "raw" fibre length measurement at a reference pose, we reasoned that an MTU would operate at a shorter normalized fibre length, and hence generate less passive force according to its passive force-length curve, if it had a longer tendon slack length. Therefore, we re-calculated each MTU's normalised fibre length at the reference pose by allowing the sarcomere length, corresponding to the measured fibre length, to vary within one standard deviation of the mean length reported by Ward et al.³¹. We then re-estimated the MTU's normalized fibre length and corresponding tendon slack length at the reference pose. Importantly, these adjustments that we made to the tendon slack lengths of the eight MTUs were not "arbitrary", but instead reflect published variability in the sarcomere length measurements across specimens, as quantified by Ward et al.³¹

In addition to modifying tendon slack lengths, we updated the optimal fibre lengths of the vastus intermedius, vastus lateralis and vastus medialis in our model to match estimates based on *in-vivo* measurements of sarcomere lengths, obtained via microendoscopy, at 50° and 110° of resting knee flexion ⁵; optimal sarcomere length was assumed to be 2.7 µm (²¹; Table 1). After making these modifications, our refined model generated net passive moments at the hip, knee and ankle that were more consistent with experimentally-derived net passive moments reported by Riener and Edrich²⁶ (Fig. 3). The three examples presented below provide an additional, indirect test of our proposed parameter values by comparing the excitation patterns of the model, as predicted by the CMC algorithm, to those predicted using Rajagopal et al.'s model and to measured EMG recordings.

Modification of the muscles' active force-generating properties

Careful examination of our initial simulations also revealed that the muscle fibre lengths of three MTUs shortened below the threshold length that defined the base of the ascending limb of the force-length curve $(0.25\ l_0^{\rm m})$ in the model. These MTUs, medial gastrocnemius, lateral gastrocnemius and semimembranosus, shortened below their threshold lengths during late upstroke of pedalling and during the mid-swing phase of running. We therefore modified the optimal fibre length, tendon slack length, attachment points and/or wrapping surfaces of these MTUs, as needed, so that the muscle fibres operated over more reasonable ranges of their force-length curves in our simulations. The optimal fibre lengths of the gastrocnemii were modified such that muscle fibres reached their optimal lengths at the ankle angles corresponding to the onset of passive force, as estimated by Hirata et al. 17 via ultrasound shear wave elastography.

Evaluation of the refined model

We used our refined model to track the same experimental data, and thus generate a new set of muscle-driven simulations during pedalling, walking and running. Data from the pedalling simulations were averaged over five crank cycles, between consecutive top-dead centres, and data from the walking and running simulations were averaged over five gait cycles, between consecutive ipsilateral foot strikes. The simulated kinematics (from CMC) tracked the smoothed kinematics (from RRA) with maximum RMSEs that were less than 5.3° and 0.5 cm for rotational DoFs and pelvis translations, respectively; maximum errors were less than 10.2° and 0.86 cm, respectively (Fig. 4). These errors are comparable to those obtained using the *intermediate* model and are slightly higher than the recommended tolerances for kinematics obtained using CMC ¹⁶; however, the highest errors were at the subtalar joint, and rotations at this joint are difficult to quantify given the resolution obtained from conventional motion capture ²⁵. The time-varying hip, knee and ankle kinematics obtained using CMC compared very favourably with the input kinematics, providing confidence that our simulations reproduced the subjects' movement dynamics (Fig. 4).

To evaluate our refined model, we compared the results predicted using the *intermediate* and *refined* models as follows. For pedalling, we compared the model-based muscle activations with the subject's measured EMG data. For walking and running, EMG data were not collected as part of the larger study; hence, we compared the predicted muscle activations with previously-reported EMG data during walking and running at equivalent speeds ^{14,24}. EMG data of each muscle was normalised to the average peak activation predicted using the two models. We also compared the net total, passive and active joint moments during pedalling, walking, and running — as predicted using both models — by summing the moments generated by the individual muscles in each model.

Results

Both sets of muscle-driven simulations that we generated, using the intermediate and refined models, had joint angles and net joint moments that were consistent with our subjects' input pedalling, walking, and running data (Fig. 4). However, the muscle activations predicted by our refined model reproduced measured EMG signals substantially better (Figs. 5-7) than

those predicted using the intermediate model, which featured the same tibiofemoral kinematics and MTU paths as the refined model, but which had different force-generating properties for 11 MTUs. Differences in the muscle activations predicted by the two models were most pronounced during the upstroke phase of pedalling (50-100% of the crank cycle), when the hip flexed more than 90° and the knee flexed more than 110°. In particular, our refined model predicted substantially lower activations than the intermediate model for the RF, BFSH, MG, and LG (Fig. 5). Our refined model also predicted lower activations than the *intermediate* model during the mid-swing phase of running, when the knee flexed more than 100° — especially for the ST, MG, LG, and TA (Fig. 6). Notably, the "excessive activations" of these muscles, as predicted by the intermediate model, were the result of coactivating flexors and extensors. For the other portions of the gait/crank cycle, and for other muscles, the timing of the predicted activations for both models were mostly consistent with the EMG signals.

As hypothesised, the anomalous co-activation of antagonist muscles predicted by our intermediate model was a result of excessive passive forces, generated by the hip and knee extensors, at the flexed limb positions. When we refined the passive properties of the gluteus maximus, the vasti, and the rectus femoris to prevent them from generating high passive forces, we found that the co-activation was greatly diminished (Figs. 5-7). For example, the net passive hip moment during the upstroke of pedalling, generated predominantly by the hip extensors, decreased from a peak of 60.5 N m, using the intermediate model, to 23.8 N m, using our refined model. The net passive knee moment during the upstroke, generated mostly by knee extensors, decreased from a peak of 36.9 N m, using the intermediate model, to 6.3 N m, using our refined model (Fig. 5). Not surprisingly, these greater net passive moments from the intermediate model were associated with the simultaneous generation of substantially greater net active moments. These "compensatory" active moments were necessarily a result of the CMC tracking algorithm, which aims to reproduce net joint moments, as determined from inverse dynamics.

We observed the simultaneous generation of greater active moments, to compensate for the greater passive moments, not only in our simulations of pedalling, but also in our simulations of walking and running when we used the intermediate model. This anomalous co-activation occurred during the early to mid-swing phase. The net passive moments, along with the co-activation, were substantially reduced when we used our refined model (Figs. 6-7). For example, the net passive knee moment during running decreased from a peak of 48.2 N m, using the intermediate model, to 8.1 N m, using our refined model. The net passive knee moment during walking decreased from a peak of 30.2 N m, using the intermediate model, to 12.3 N m, using our refined model.

The changes we made to the optimal fibre lengths and tendon slack lengths of the MG, LG and SM in our refined model successfully prevented these MTUs from shortening below $0.25 \, l_0^{\, m}$ in the tasks simulated here; this fibre length represents the base of the ascending limb of the force-length curve in the Hill-type model proposed by Millard et al.²³ (Fig. 8). For example, when we used the refined model to simulate pedalling, the fibres of the MG and LG did not shorten below $0.37 \, l_0^{\, m}$ at any time in the crank cycle. By contrast, when we used the intermediate model, the MG and LG fibres shortened below $0.25 \, l_0^{\, m}$ at about 80%

of the crank cycle and did not re-lengthen onto the ascending limb of the force-length curve until about 10% of the next cycle. Similarly, when we used the intermediate model to simulate running, the MG fibres shortened below the base of the force-length curve between 60-65% of the gait cycle, but this did not occur when we used the refined model.

Discussion

Access to high-quality simulation software, such as OpenSimTM, has allowed researchers to share detailed musculoskeletal models with colleagues worldwide. Given the resources and effort required to develop new models suitable for multibody simulations, e.g. by generating 3D reconstructions of bone geometry from image data or statistical shape models (e.g. ^{7,35}), by characterising *in-vivo* joint kinematics (e.g. ¹³), or by measuring muscle sarcomere lengths (e.g. ^{5,31}), establishing an open-source library of generic "off-the-shelf" models is unquestionably appealing. However, even the most up-to-date models have limitations that are often non-trivial for users to identify — yet may need to be addressed before the model can be applied to investigate a new research question ¹⁶.

The refined lower extremity model described and tested in this study was motivated, in large part, by inconsistencies that we uncovered when attempting to use an existing model to simulate pedalling. In particular, our preliminary simulations predicted the co-activation of antagonist muscles, which was inconsistent with measured EMG recordings. We hypothesised that this co-activation could be resolved if passive forces generated by the hip and knee extensors were diminished. To test this hypothesis, we created a refined version of the model that has knee moment arms and net passive hip, knee and ankle joint moments that are more consistent with experimental data, over a broader range of hip and knee angles, than the existing model. We ran muscle-driven simulations of pedalling, walking and running using both versions of the model, and we demonstrated that the muscle activation patterns predicted by our refined model are more consistent with subjects' measured EMG signals than the activation patterns predicted by the existing model. We also confirmed that the net passive moments generated by the hip and knee extensors are dramatically decreased in the simulations using the refined model (Figs. 5-7).

We considered several potential strategies to reduce the high passive forces generated by the hip and knee extensors in the existing model. Arguably, the simplest approach might have been to modify the normalised passive fibre force-length curve for each of the problematic MTUs, for example, by increasing the passive fibre strain at peak isometric force ²³. In both the existing model and in our refined model, muscle fibres transmit a passive force equal to the muscle's peak isometric force when they are stretched 60% beyond optimal fibre length. However, we would have needed to allow muscle fibres to stretch nearly 120% beyond optimal fibre length to obtain the necessary decreases in passive hip and knee moments generated during the upstroke phase of pedalling. Presently, experimental justification for such an increase is lacking, so we explored other options.

We also considered increasing, within limits, the optimal fibre lengths of the problematic MTUs. However, these lengths are based on the best-available measurements of sarcomere lengths, so we were hesitant to alter them. We did however, update the optimal fibre lengths

of the VI, VL and VM in our refined model to match estimates based on recently published *in-vivo* measurements of sarcomere lengths obtained via microendoscopy ⁵. We also updated the optimal fibre lengths of the MG and LG to match estimates of fibre length at ankle angle at which passive forces began to be detected ¹⁷.

Ultimately, we decided to increase tendon slack lengths for eight MTUs in the model that generated substantial passive force during our preliminary simulations. These modifications were not made in an arbitrary manner; rather, they were based on our preliminary analyses and other information available. For instance, we limited the changes in tendon slack length to be less than the expected variation reported by Rajagopal et al.²⁵ (Table 1), and verified that our refined model generated net passive moments at the hip, knee and ankle that were more consistent with experimentally measured net passive moments²⁶ than those predicted using the existing model (Fig. 3). We also showed, for walking, that our refined model generated net passive moments at the hip, knee and ankle that were more consistent with previously reported net passive moments ³² than those predicted using the existing model, especially during swing phase.

Despite these improvements, our refined model still has some important limitations. First, while the knee moment arms of the SM and ST compare favourably with experimentally measured moment arms over 0-90° of knee flexion, the moment arms are too small at the more extreme ranges of knee flexion (Suppl. Fig. S1). Additional work is required to characterise the musculotendon paths of the SM and ST over the functional range of knee flexion. By contrast, knee moment arms of the vasti, biceps femoris and gastrocnemii in our refined model are notably improved (Fig. 1 and Suppl. Fig. S1).

Second, while the net passive moments of the hip extensors in our refined model approximate published experimental data better than the existing model (Fig. 3), the model overestimates the net passive moments at hip flexion greater than about 50°. A plausible explanation for this discrepancy is that the length-tension properties of relevant tendons are not included in the model. For example, in both models used in this study, the three MTUs of the gluteus maximus contain a "rigid" tendon ²⁵. Yet, over 50% of the gluteus maximus, by mass, inserts into the iliotibial band; this fascial structure is more compliant than tendon and is certainly not rigid ¹⁰. Hence, it is likely that the muscle fibre length changes of the gluteus maximus are overestimated in our model, possibly contributing to the observed high passive hip moments. More sophisticated models of the gluteus maximus have been developed (e.g. ¹⁰), and need to be adapted for use in muscle-driven simulations.

Lastly, although our updates to the active force-generating properties of the gastrocnemii were successful in preventing these muscles from shortening past 0.25 $l_0^{\rm m}$ in our simulations, the predicted fibre excursions of these muscles — during pedalling, walking and running — remain far greater than the excursions measured *in-vivo* using ultrasonography (e.g. ^{9,20}). In our model, as in other OpenSimTM models, each MTU is represented by a one-dimensional path, and all fibres within the muscle are assumed to change length equally. However, the pennate fibres within the gastrocnemii have a distribution of lengths ³¹ and moment arms, and our model may overestimate the fibre excursions, in part, because it ignores these distributions (e.g., ³). In any case, further

improvements to the muscles' 3D geometric paths are required before we can be reasonably confident in the predicted operating regions of the muscle fibres on their force-length and force-velocity curves.

In conclusion, we concur with Rajagopal et al. 25 that testing a musculoskeletal model in the context of its intended use is a critical step for any simulation study. Frequently, muscle activations predicted by muscle-driven simulations are evaluated against measured EMG signals. When discrepancies occur, they are usually attributed to errors in the optimisation algorithm or a poorly-formulated cost function — and not to flaws in the underlying model, since versions of the existing model have been widely shared and iteratively improved over the last 30 years. However, our study shows that the same optimisation algorithm, tracking the same kinematics, can yield different muscle activation patterns depending on the underlying musculoskeletal model, or more specifically, depending on just a few parameters that scale a normalised muscle model to individual MTUs. In this study, we identified muscles that generated implausible passive forces during pedalling, walking and running, leading to compensatory active forces and anomalous co-activation of antagonist muscles, which were inconsistent with measured EMG data. Our proposed refinements to the model extend the model's functional range of motion, making it more applicable to biomechanical studies of springing, cycling, rowing and other movements involving substantial hip and knee flexion. Certainly, we encourage others to make additional refinements to the model and share them with the community. Our model is available from SimTK.org (https:// simtk.org/projects/model-high-flex).

Supplementary Material

Refer to Web version on PubMed Central for supplementary material.

Acknowledgments

We thank Taylor Dick, Sidney Morrison and Glen Lichtwark for their assistance in collecting and post-processing the experimental data used in this study, and we are grateful to Andy Biewener and Carolyn Eng for helpful discussions. Funding for this work was provided by the National Institutes of Health Grant 2R01AR055648.

References

- Arnold EM, Hamner SR, Seth A, Millard M, Delp SL. How muscle fiber lengths and velocities affect muscle force generation as humans walk and run at different speeds. J Exp Biol. 2013; 216:2150–2160. [PubMed: 23470656]
- Arnold EM, Ward SR, Lieber RL, Delp SL. A model of the lower limb for analysis of human movement. Ann Biomed Eng. 2010; 38:269–279. [PubMed: 19957039]
- 3. Blemker SS, Delp SL. Rectus femoris and vastus intermedius fiber excursions predicted by three-dimensional muscle models. J Biomech. 2006; 39:1383–1391. [PubMed: 15972213]
- 4. Buford WL, J J, Ivey FM, Malone JD, Patterson RM, Peare GL, Nguyen DK, Stewart AA. Muscle balance at the knee Moment arms for the normal knee and the ACL-minus knee. IEEE Trans Rehabil Eng. 1997; 5:367–379. [PubMed: 9422462]
- 5. Chen X, Sanchez GN, Schnitzer MJ, Delp SL. Changes in sarcomere lengths of the human vastus lateralis muscle with knee flexion measured using in vivo microendoscopy. J Biomech. 2016; 49:2989–2994. [PubMed: 27481293]

Delp SL, Anderson FC, Arnold AS, Loan P, Habib A, John CT, Guendelman E, Thelen D.
 OpenSim: Open-source software to create and analyze dynamic simulations of movement. IEEE Trans Biomed Eng. 2007; 54:1940–1950. [PubMed: 18018689]

- Delp SL, Loan JP, Hoy MG, Zajac FE, Topp EL, Rosen JM. An interactive graphics-based model of the lower extremity to study orthopaedic surgical procedures. IEEE Trans Biomed Eng. 1990; 37:757–67. [PubMed: 2210784]
- 8. Dick TJM, Arnold AS, Wakeling JM. Quantifying Achilles tendon force in vivo from ultrasound images. J Biomech. 2016; 49:3200–3207. [PubMed: 27544621]
- 9. Dick TJM, Biewener AA, Wakeling JM. Comparison of human gastrocnemius forces predicted by Hill-type muscle models and estimated from ultrasound images. J Exp Biol. 2017:778–782.
- 10. Eng CM, Arnold AS, Lieberman DE, Biewener AA. The capacity of the human iliotibial band to store elastic energy during running. J Biomech. 2015; 48:3341–3348. [PubMed: 26162548]
- 11. Fregly BJ, Besier TF, Lloyd DG, Delp SL, Banks SA, Pandy MG, D'Lima DD. Grand challenge competition to predict in vivo knee loads. J Orthop Res. 2012; 30:503–513. [PubMed: 22161745]
- Friederich JA, Brand RA. Muscle fiber architecture in the human lower limb. J Biomech. 1990;
 23:91–95. [PubMed: 2307696]
- 13. Guan S, Gray HA, Keynejad F, Pandy MG. Mobile biplane x-ray imaging system for measuring 3D dynamic joint motion during overground gait. IEEE Trans Med Imaging. 2016; 35:326–336. [PubMed: 26316030]
- 14. Hamner SR, Delp SL. Muscle contributions to fore-aft and vertical body mass center accelerations over a range of running speeds. J Biomech. 2013; 46:780–787. [PubMed: 23246045]
- 15. Handsfield GG, Meyer CH, Hart JM, Abel MF, Blemker SS. Relationships of 35 lower limb muscles to height and body mass quantified using MRI. J Biomech. 2014; 47:631–638. [PubMed: 24368144]
- Hicks JL, Uchida TK, Seth A, Rajagopal A, Delp SL. Is my model good enough? Best practices for verification and validation of musculoskeletal models and simulations of movement. J Biomech Eng. 2015; 137:1–24.
- 17. Hirata K, Kanehisa H, Miyamoto-Mikami E, Miyamoto N. Evidence for intermuscle difference in slack angle in human triceps surae. J Biomech. 2015; 48:1210–1213. [PubMed: 25682539]
- Lai A, Lichtwark GA, Schache AG, Lin YC, Brown NAT, Pandy MG. In vivo behavior of the human soleus muscle with increasing walking and running speeds. J Appl Physiol. 2015; 118:1266–1275. [PubMed: 25814636]
- Lai A, Schache AG, Brown NAT, Pandy MG. Human ankle plantar flexor muscle-tendon mechanics and energetics during maximum acceleration sprinting. J R Soc Interface. 2016; 13:20160391. [PubMed: 27581481]
- Lichtwark GA, Bougoulias K, Wilson AM. Muscle fascicle and series elastic element length changes along the length of the human gastrocnemius during walking and running. J Biomech. 2007; 40:157–164. [PubMed: 16364330]
- 21. Lieber RL, Loren GJ, Fridén J. In vivo measurement of human wrist extensor muscle sarcomere length changes. J Neurophysiol. 1994; 71:874–81. [PubMed: 8201427]
- 22. Liu MQ, Anderson FC, Schwartz MH, Delp SL. Muscle contributions to support and progression over a range of walking speeds. J Biomech. 2008; 41:3243–3252. [PubMed: 18822415]
- 23. Millard M, Uchida T, Seth A, Delp SL. Flexing computational muscle: modeling and simulation of musculotendon dynamics. J Biomech Eng. 2013; 135:1–11.
- 24. Perry, J., Burnfield, JM. Gait analysis: Normal and pathological function. New Jersey: Slack Incorporated; 2010. p. 1-551.
- 25. Rajagopal A, Dembia C, DeMers M, Delp D, Hicks J, Delp S. Full body musculoskeletal model for muscle-driven simulation of human gait. IEEE Trans Biomed Eng. 2016; 63:1–1.
- 26. Riener R, Edrich T. Identification of passive elastic joint moments in the lower extremities. J Biomech. 1999; 32:539–544. [PubMed: 10327008]
- 27. Thelen DG, Anderson FC. Using computed muscle control to generate forward dynamic simulations of human walking from experimental data. J Biomech. 2006; 39:1107–1115. [PubMed: 16023125]

 Von Tscharner V. Intensity analysis in time-frequency space of surface myoelectric signals by wavelets of specified resolution. J Electromyogr Kinesiol. 2000; 10:433–445. [PubMed: 11102846]

- 29. Wakeling JM, Horn T. Neuromechanics of muscle synergies during cycling. J Neurophysiol. 2009; 101:843–854. [PubMed: 19073812]
- 30. Walker PS, Rovick JS, Robertson DD. The effects of knee brace hinge design and placement on joint mechanics. J Biomech. 1988; 21
- 31. Ward S, Eng C, Smallwood L, Lieber R. Are current measurements of lower extremity muscle architecture accurate? Clin Orthop Relat Res. 2009; 467:1074–1082. [PubMed: 18972175]
- 32. Whittington B, Silder A, Heiderscheit B, Thelen DG. The contribution of passive-elastic mechanisms to lower extremity joint kinetics during human walking. Gait Posture. 2008; 27:628–634. [PubMed: 17928228]
- 33. Wickiewicz TL, Roy RR, Powell PL, Perrine JJ, Edgerton VR. Muscle architecture and force-velocity relationships in humans. J Appl Physiol. 1984; 57:435–443. [PubMed: 6469814]
- 34. Zajac FE. Muscle and tendon: Properties, models, scaling, and application to biomechanics and motor control. Crit Rev Biomed Eng. 1989; 17:359–411. [PubMed: 2676342]
- 35. Zhang J, Besier TF. Accuracy of femur reconstruction from sparse geometric data using a statistical shape model. Comput Methods Biomech Biomed Engin. 2017; 20:566–576. [PubMed: 27998170]

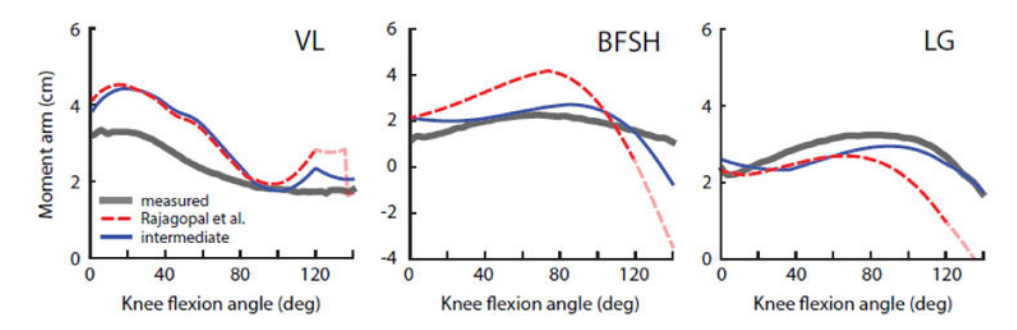


Figure 1.

Knee moment arms of the vastus lateralis (VL), biceps femoris short head (BFSH) and lateral gastrocnemius (LG) as predicted by Rajagopal et al.'s model²⁵ and by our intermediate model after updating the tibiofemoral translations and MTU paths. Moment arms predicted by the models are compared with measured moment arms reported by Buford et al.⁴ from tendon excursion experiments. Note that the moment arms for Rajagopal et al.'s model²⁵ are extrapolated for knee angles greater than 120° (lighter dotted lines). The moment arms for our refined model are identical to those predicted by the intermediate model. Knee moment arms for all MTUs spanning the knee are provided in Suppl. Fig. S1.

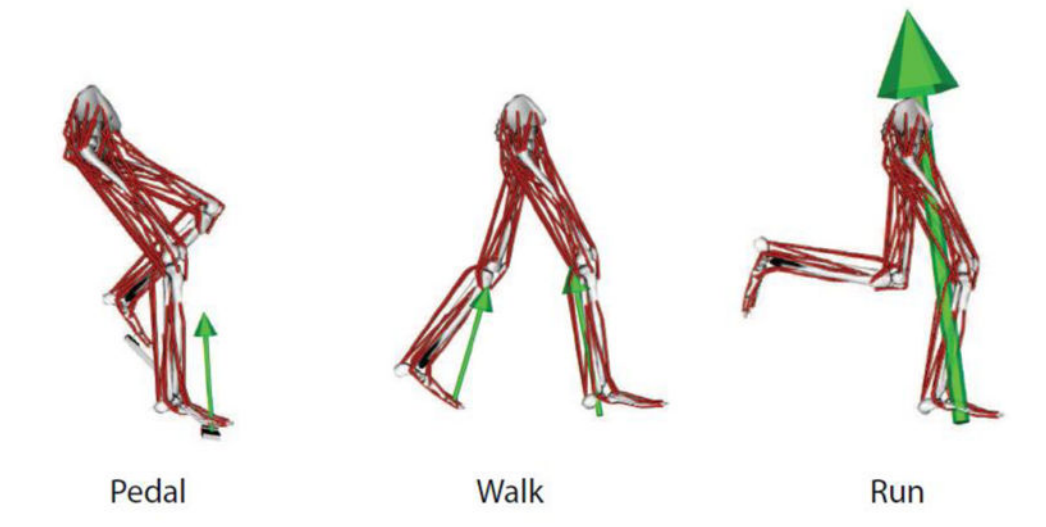


Figure 2.Sagittal-plane images of the refined, subject-specific models during pedalling, walking and running. Each arrow represents the magnitude and direction of the resultant reaction force vector. Data from the right leg were analysed for this study.

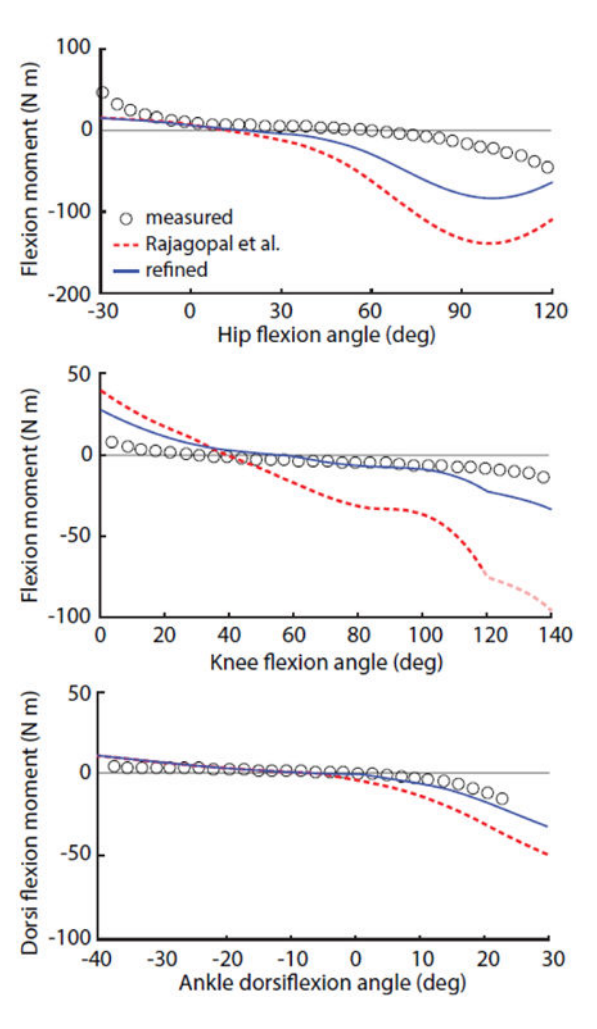


Figure 3.

Net passive moments generated by MTUs crossing the hip, knee and ankle, both before (Rajagopal et al., dotted) and after (refined, solid) modifying the passive force-generating properties of eight MTUs. Hip moments were computed with the knee flexed 10°, knee moments were computed with the hip flexed 70°, and ankle moments were computed with the knee flexed 80°. Passive moments generated by the models are compared with experimental data reported by Riener and Edrich²⁶.

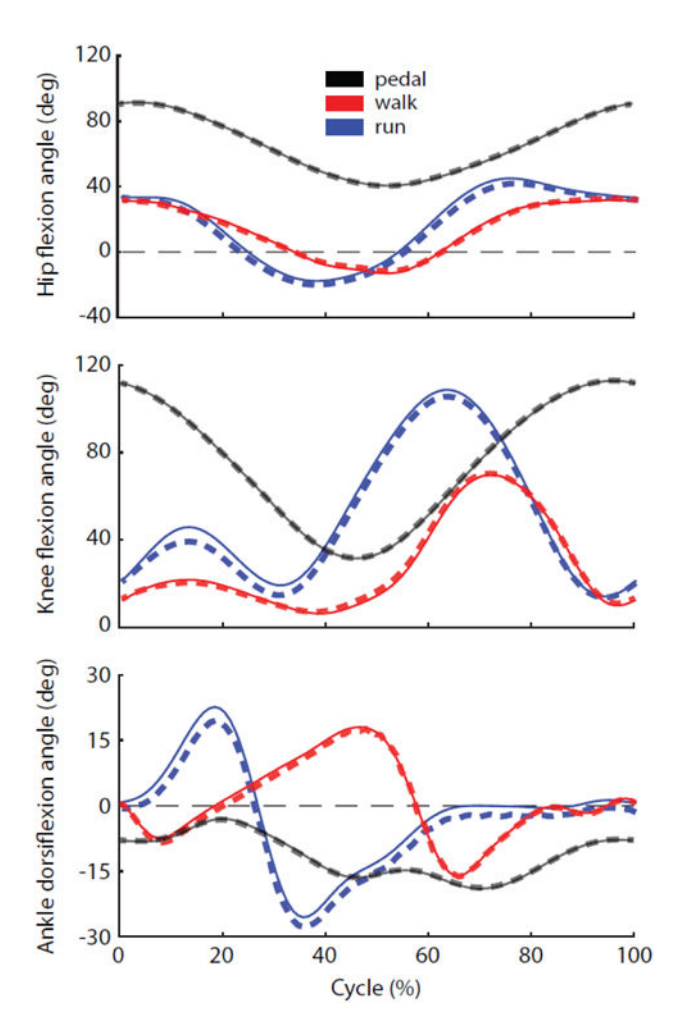


Figure 4.Hip, knee and ankle angles of our refined model, computed using RRA (solid) and tracked using CMC (dashed) during pedalling, walking and running. Positive hip, knee and ankle angles represent hip flexion, knee flexion and ankle dorsiflexion, respectively.

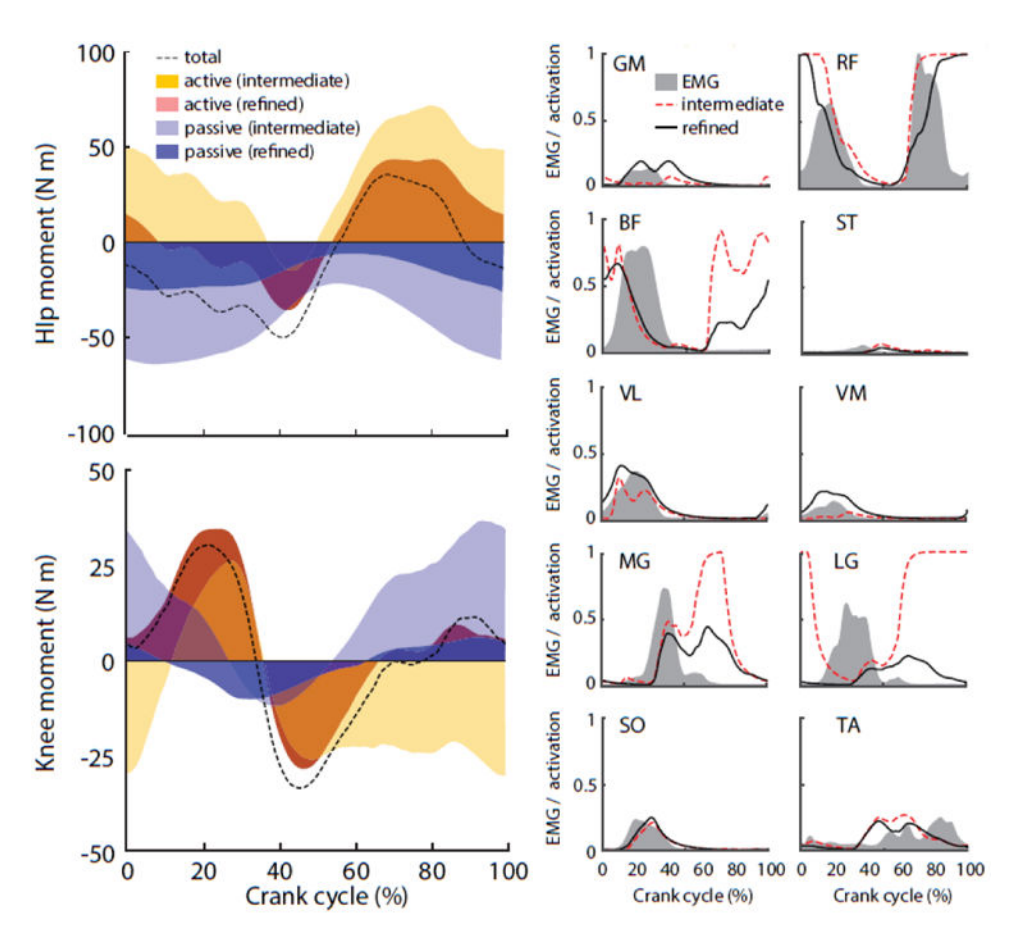


Figure 5.

Net total moments (dotted lines) and net passive and active moments (shaded regions) generated by MTUs crossing the hip and knee, as estimated from muscle-driven simulations of pedalling (left). Net moments estimated using our refined model are compared to the moments estimated using our intermediate model. Muscle activation patterns (right) predicted from the refined model (solid black lines) are compared with the activation patterns predicted from the intermediate model (dotted red lines) and with measured EMG activity (shaded regions) for ten lower limb muscles during pedalling. The ten muscles include gluteus maximus (GM), rectus femoris (RF), biceps femoris long head (BF), semitendinosus (ST), vastus lateralis (VL), vastus medius (VM), medial gastrocnemius (MG), lateral gastrocnemius (LG), soleus (SO) and tibialis anterior (TA). Predicted muscle activations were normalised from no activation (0) to full activation (1). EMG activity was normalised to the peak activation averaged for the two models.

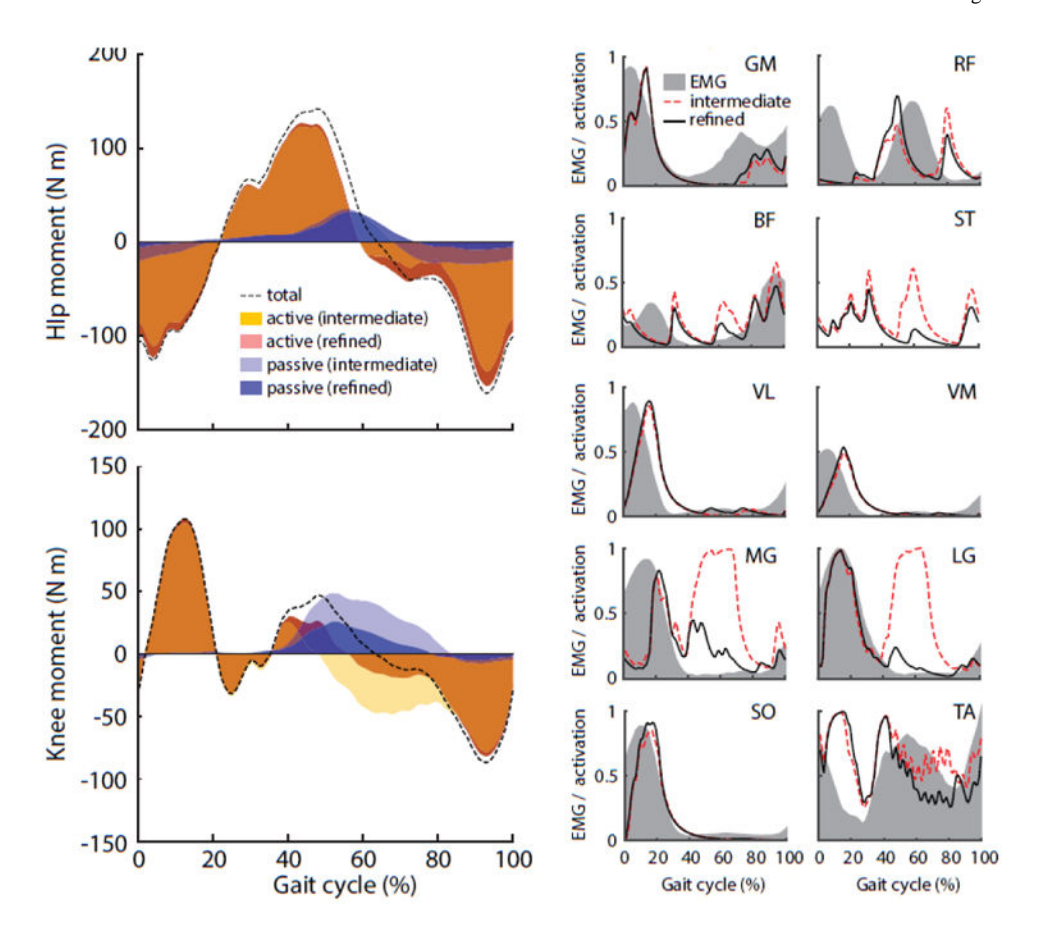


Figure 6.

Net total moments (dotted lines) and net passive and active moments (shaded regions) generated by MTUs crossing the hip and knee, as estimated from muscle-driven simulations of running at 4 m s⁻¹ (left). Net moments estimated using our refined model are compared to the moments estimated using our intermediate model. Muscle activation patterns (right) predicted from the refined model (solid black lines) are compared with the activation patterns predicted from the intermediate model (dotted red lines) and with published EMG activity (shaded regions) for ten lower limb muscles during running ¹⁴. The ten muscles include gluteus maximus (GM), rectus femoris (RF), biceps femoris long head (BF), semitendinosus (ST), vastus lateralis (VL), vastus medius (VM), medial gastrocnemius (MG), lateral gastrocnemius (LG), soleus (SO) and tibialis anterior (TA). Predicted muscle activations were normalised from no activation (0) to full activation (1). EMG activity was normalised to the peak activation averaged for the two models. Note that Hamner et al. ¹⁴ did not report EMG data for the semitendinosus.

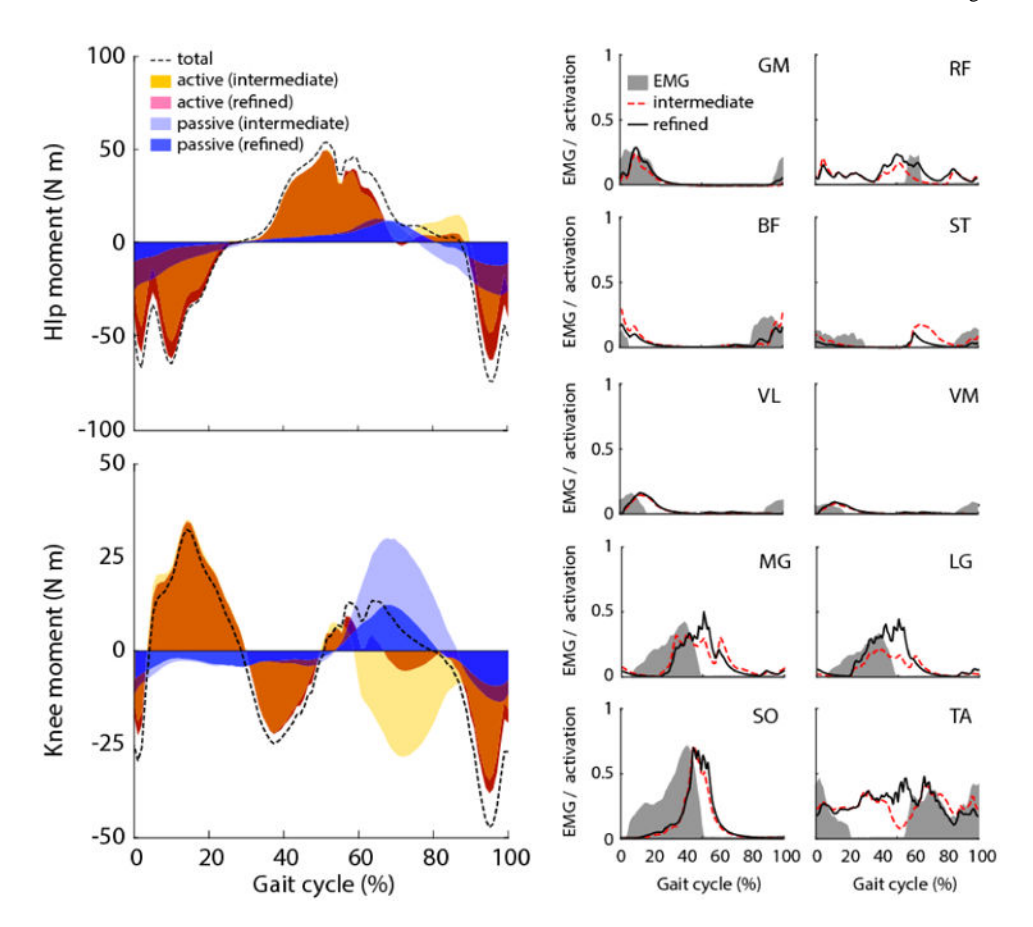


Figure 7.

Net total moments (dotted lines) and net passive and active moments (shaded regions) generated by MTUs crossing the hip and knee, as estimated from muscle-driven simulations of walking at 1.4 m s⁻¹ (left). Net moments estimated using our refined model are compared to the moments estimated using our intermediate model. Muscle activation patterns (right) predicted from the refined model (solid black lines) are compared with the activation patterns predicted from the intermediate model (dotted red lines) and with published EMG activity (shaded regions) for ten lower limb muscles during walking ²⁴. The ten muscles include gluteus maximus (GM), rectus femoris (RF), biceps femoris long head (BF), semitendinosus (ST), vastus lateralis (VL), vastus medius (VM), medial gastrocnemius (MG), lateral gastrocnemius (LG), soleus (SO) and tibialis anterior (TA). Predicted muscle activations were normalised from no activation (0) to full activation (1). EMG activity was normalised to the peak activation averaged for the two models.

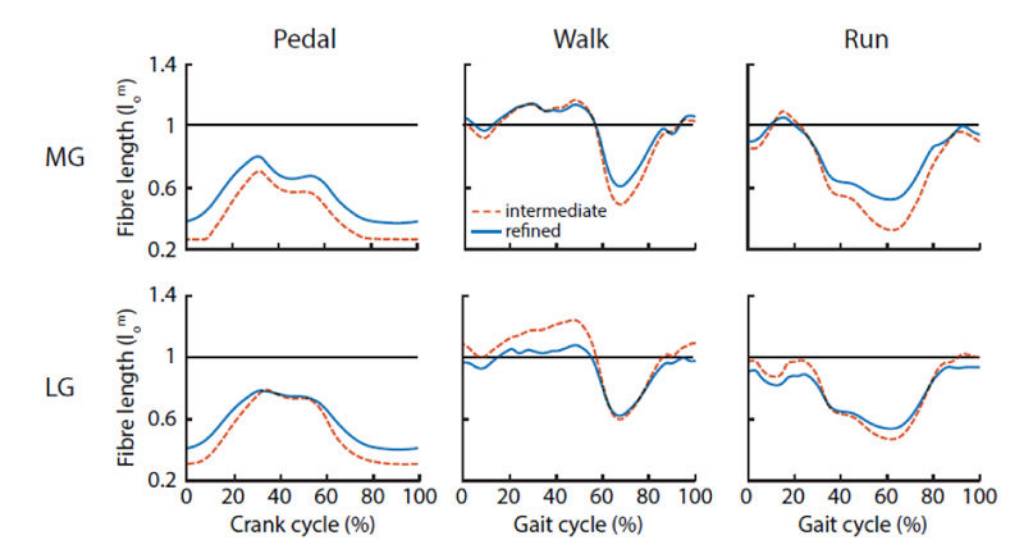


Figure 8.

Normalised fibre lengths of the medial gastrocnemius (MG) and lateral gastrocnemius (LG) during pedalling, walking and running as estimated using our refined model (solid lines) and our intermediate model (dashed lines). Fibre lengths are normalised to optimal fibre length.

Table 1Proposed updates to the optimal fibre lengths and tendon slack lengths to simulate pedalling, walking, and running.

Muscle	Optimal fibre length (cm)		Tendon slack length (cm)	
	Rajagopal et al.* †	Refined	Rajagopal et al. *†	Refined
Gastrocnemius lateral head	5.9 ± 1.0	6.9	37.6 ± 1.1	37.4
Gastrocnemius medial head	5.1 ± 1.0	5.9	39.9 ± 1.1	38.7
Gluteus maximus (Superior)	14.7 ± 2.4	NC§	4.9 ± 4.0	8.7
Gluteus maximus (Middle)	15.7 ± 2.6	NC	6.8 ± 4.4	10.9
Gluteus maximus (Inferior)	16.7 ± 2.7	NC	7.0 ± 4.9	10.3
Rectus femoris	7.6 ± 1.3	NC	44.9 ± 1.4	45
Semimembranosus	6.9 ± 1.8	8.6	34.8 ± 2.1	33.5
Soleus	4.4 ± 1.0	NC	27.7 ± 1.0	28.1
Vastus intermedius	9.9 ± 2.0	11.7	20.2 ± 2.3	20.5
Vastus lateralis	9.9 ± 1.8	11.7	22.1 ± 1.9	NC
Vastus medialis	9.7 ± 2.3	11	20.0 ± 2.8	20.8
Vastus lateralis	9.9 (1.8)	11.7	22.1 (1.9)	22.1
Vastus medialis	9.7 (2.3)	11	20.0 (2.8)	20.8

^{*} Mean parameters with their expected variation (\pm SD) as reported by Rajagopal et al. ²³

 $[\]dot{\vec{r}}_{Values}$ for the intermediate model are identical to those specified by Rajagopal et al. 23